Regular article

Colloidal-quantum-dot-in-perovskite nanowires

Ruili Wang[a,c,d], Fei Wang[a], Wenjia Zhou[a,*], James Z. Fan[b], F. Pelayo García de Arquer[b], Kaimin Xu[a], Edward H. Sargent[b,*], Zhijun Ning[a,*]

[a] School of Physical Science and Technology, ShanghaiTech University, Shanghai 201210, China
[b] Department of Electrical and Computer Engineering, University of Toronto, 10 King's College Rd, Toronto, Ontario M5S 3G4, Canada
[c] Shanghai Institute of Ceramic, Chinese Academy of Sciences, Shanghai 200050, China
[d] School of Chemistry and Chemical Engineering, University of Chinese Academy of Sciences, Beijing 100049, China

ABSTRACT

Colloidal quantum dots are materials of interest in infrared detection – a consequence of their near-infrared light harvesting capability, tunable bandgap, and solution-processing. Herein we develop a quantum-dot-in-perovskite-nanowire consisting of PbS quantum dots embedded inside MAPbI$_3$ nanowires. The kinetics of perovskite nanowire growth were tracked. We found that N,N-dimethylformamide induced the formation of perovskite nanowires, and that their growth was accelerated upon PbS quantum dot inclusion. We then used this nanocomposite to fabricate photodetectors that showed a light response from the visible to near infrared region up to 940 nm. Finally, a flexible photodetector was fabricated on a polyethylene terephthalate substrate.

1. Introduction

Infrared (IR) detection is important for technologies such as night vision, health diagnosis, proximity detection, and time-of-flight ranging [1–4]. Traditional IR detectors rely on vacuum processed materials, such as InGaAs and CdHgTe, which depend on expensive fabrication process [5,6]. In recent years, solution-processed colloidal quantum dots (QDs) have emerged as promising IR light detecting materials owing to their excellent near-infrared (NIR) light harvesting capabilities, tunable bandgap, and low cost [7–10]. The performance of QD based photodetectors was significantly improved due to recent achievements in QD surface optimization and device structure engineering, e.g. introducing halide ligands to increase carrier mobility and forming n-type QD films [11,12], building graded device architectures and Schottky junction device [13–15].

Organic-inorganic hybrid metal halide perovskites have attracted attention in optoelectronic devices for their tunable bandgap, solution processability, and micron-scale exciton diffusion lengths [16–18]. They are ideal matrix materials for transporting carriers into QDs because (1) perovskites can epitaxially grow on QDs because both materials share similar crystal lattice constants and (2) the excellent carrier transporting capabilities of perovskites allow for fast carrier transport between both materials. Therefore, the combination of perovskites and QDs present a promising material platform to build IR light emitting diodes and photodetectors [19,20].

Recently, photodetectors based on one-dimensional perovskite nanowires (NWs) have received special attention for their excellent sensitivity and flexibility [21]. Deng et al. fabricated a photodetector with ultrahigh-responsivity, while Gao et al. prepared a photodetector with high detectivity and polarization sensitivity from single crystalline perovskite NWs [22,23]. Moreover, perovskite nanowire photodetectors were also fabricated on flexible substrates [24].

Herein, we fabricated MAPbI$_3$ perovskite NWs with embedded PbS QDs. The MAPbI$_3$ perovskite NWs act as the host transporting material and PbS QDs as the IR light harvesting material. We studied the influence of solvents on nanowire growth, and performed characterizations such as transmission electron microscopy (TEM) and X-ray diffraction (XRD) to confirm the formation of the nanocomposite structure. Photodetectors based on this nanocomposite showed photoresponse in both visible and NIR regions. Finally, as a proof of concept, we demonstrate a flexible photodetector using QD-in-perovskite nanowires.

2. Experimental methods

2.1. Materials purchase

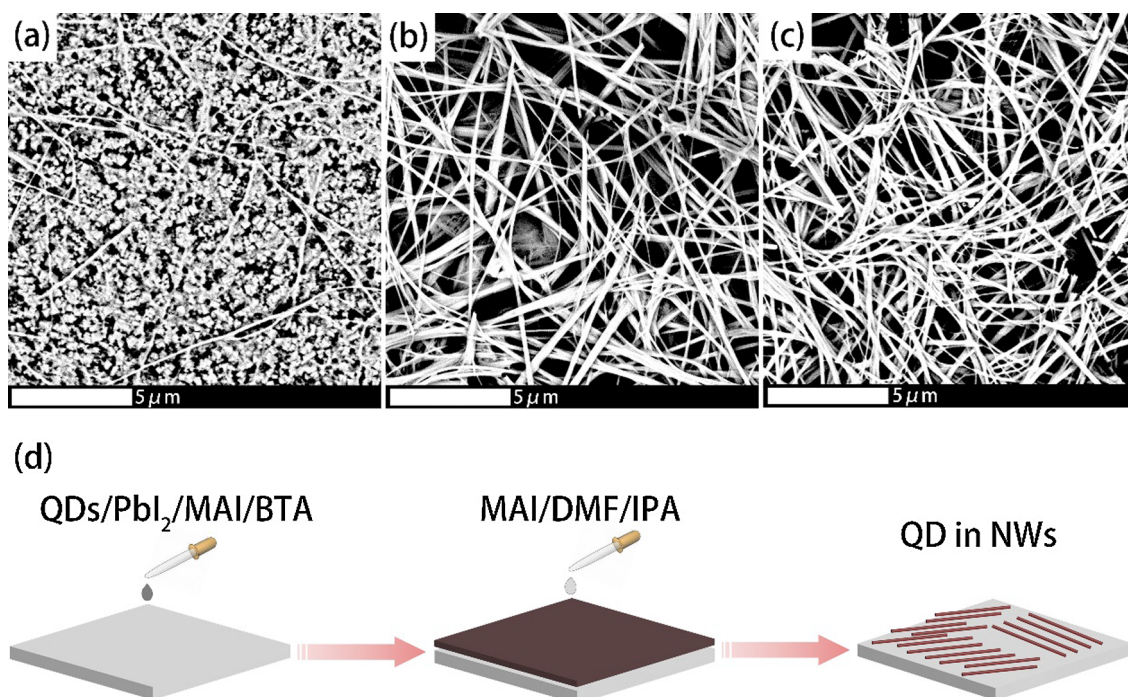Lead oxide yellow (PbO, 99.99%, metals basis), lead iodide

---

Fig. 1. The influence of QD ratios on nanowire growth, top-view SEM images of nanowire films with PbS QDs to PbI_2 mass ratio as (a) 0:1, (b) 1:5, (c) 1:3, (d) Schematic of the fabrication process of QD-in-perovskite NWs.

(PbI_2, 98%), oleic acid (OA, AR), 1-octadecene (ODE, > 90%, GC), n-octane (96%), N, N-dimethylformamide (DMF, 99.5%, AR), n-butylamine (BTA, 98%, AR), isopropanol (IPA, 99.5%, GC) were purchased from Aladdin. Hexamethyldisilathiane (TMS, synthesis grade) was purchased from Aldrich-sigma. Hexane (AR), acetone (AR), and toluene (AR) were purchased from Sinopharm. Methylammonium iodide (MAI, 99%) was purchased from Solarmer.

2.2. Dot-in-nanowire growth

PbS QDs were synthesized by the typical hot injection method and post treated via halide ligands. The long ligands on the QDs were exchanged to iodide via solution phase ligand exchange [25]. To prepare the QD-in-perovskite nanowires, 100 mg of PbS QDs were dissolved in a solution containing 100 mg of PbI_2 (with one quarter weight ratio of MAI) dissolved in butylamine. This solution was spin coated at 2500 rpm onto a polyethylene terephthalate (PET) film with gold (Au) contacts followed by annealing at 70 °C for 10 min in ambient conditions (relative humidity ∼ 50%). Then, the films were soaked in isopropanol (MAI/DMF/IPA, 60 mg/300 μL/5 mL) for six minutes. Finally, the film was annealed at 70 °C for 10 min.

2.3. Characterization

The optical properties were characterized by a UV–Vis spectrometer (Cary 5000, Aligent) and a photoluminescence spectrometer (Fluorolog-3, Horiba). The morphology was measured by scanning electron microscopy (SEM) (JSM-6010PLUS/LA and JSM-7800F Prime). X-ray diffraction was measured on a D2 Phaser desktop XRD. Transmission electron microscope was taken by the FEI Tecnai G2 F20.

The I-V curve and response time were measured with a Keithley 2400 source meter.

3. Results and discussion

PbS QDs with exciton peaks around 950 nm were synthesized via a hot injection method by using lead oleate and hexamethyldisilathiane as precursors. The long ligands on the PbS QD surface were exchanged by iodide ligands, during which PbI_2 and MAI dissolved in N, N-dimethylformamide were mixed with PbS QDs dissolved in octane. Exchange of halide ligands allows epitaxy growth of perovskite matrix on them, and short halide ligands facilitates carriers extraction from QDs to matrix [26].

The dot-in-nanowire nanocomposite was prepared through a two-step method (Fig. 1d). In the first step, the PbS QDs were dispersed in butylamine containing PbI_2 with one quarter weight ratio of MAI, and subsequently spin-coated on a substrate. In the second step, the film was soaked in an IPA/DMF/MAI solution to convert PbI_2 into $MAPbI_3$. PbS QDs play important roles in the growth of NWs by acting as seeds to induce formation of perovskite nanowires. This is possible because both materials share similar lattice constants. Without the presence of QDs, few NWs were grown and bulk perovskites were formed (Fig. 1a–c). The optimized volume ratio for nanowire growth is 28% QDs: perovskites, closely matching a previous report [27].

We investigated the effect of nanowire growth with different solvent compositions. Different ratios of DMF: IPA were studied (Fig. 2a–c). Increasing the DMF content promotes the formation of the intermediate structure $MAI-PbI_2-DMF$, which speeds up the growth of NWs [28]. We tracked the nanowire growth process by SEM. In the beginning, NWs grew on the film surface since bulk materials were observed on the bottom. After three minutes, the bulk perovskites disappeared and NWs formed homogeneously (Fig. 2d–f). The optimized time for nanowire
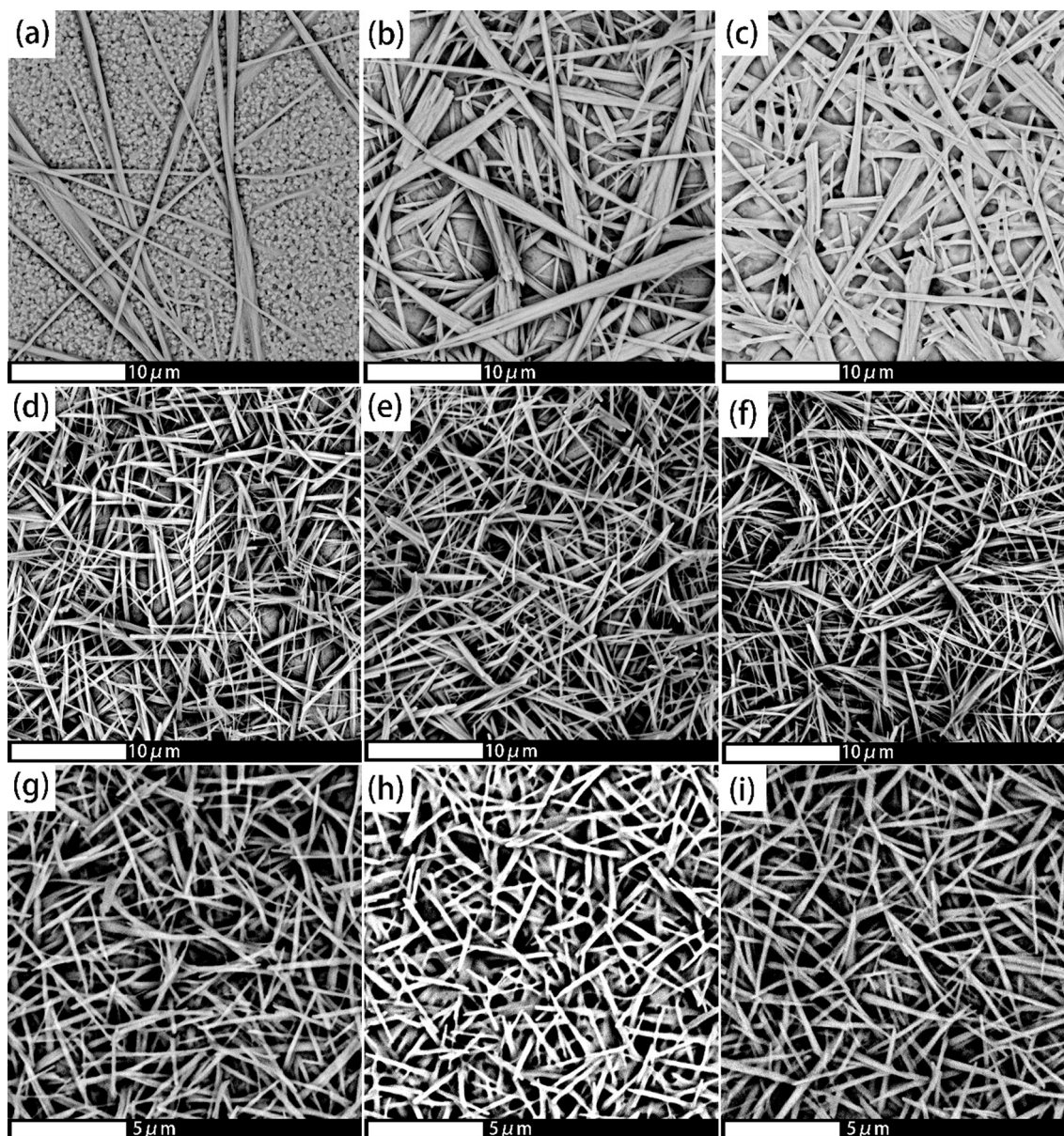
Fig. 2. Top-view SEM images of nanowire films with different DMF volumes (a) 100 μL, (b) 200 μL, (c) 300 μL in a MAI/IPA solution. SEM images showing different MAI/DMF/IPA soaking times, (d) 1 min, (e) 3 min, (f) 6 min. SEM images showing NW films grown on different substrates (g) glass, (h) NiO film, (i) polyetherimide (PEI) film. The mass ratio of PbS QDs to PbI$_2$ is 1:1 during nanowire growth.

growth was six minutes. The nanowire morphology was unaffected when grown on different substrates such as glass, NiO, or PEI films (Fig. 2g–i).

We then studied the photophysical properties of the prepared films. Fig. 3a shows the absorption spectra of PbS QD films, MAPbI$_3$ NWs, and QDs in NWs. The dot-in-nanowire film shows characteristic absorption peaks of both MAPbI$_3$ at ~780 nm and PbS QDs at ~950 nm, indicating the presence of both materials. The XRD spectrum of QDs in NWs is shown in Fig. 3b. The main diffraction peaks at 14.2°, 20.1°, 23.6°, 24.6°, 31.9°, 35.3° can be ascribed to the (1 1 0), (1 1 2), (2 1 1), (2 0 2), (2 1 3), (3 1 2) planes of MAPbI$_3$ [29,30], while the XRD peak at 30.4° is attributed to the (2 0 0) plane of PbS QDs. The high-resolution transmission electron microscopy (HRTEM) images of

a dot-in-nanowire are shown in Fig. 3(c) and (d). Small black dots with an inter planar spacing of 0.29 nm derived from the (2 0 0) plane of PbS QDs were observed (Fig. 3c) [31]. However, no lattice spacing belonging to MAPbI$_3$ was observed, possibly due to the quick decomposition of perovskite under electron beam. The inter-plane spacing of 0.39 nm could be attributed to the (0 1 1) plane for PbI$_2$ (JCPDS#73-1286). Energy-dispersive X-ray spectroscopy (EDS) was employed to verify the composition of dot-in-perovskite NWs by mapping the element distribution (Fig. 4). Homogeneous distribution of lead and sulfide elements was found, indicating QDs were well dispersed in NWs.

The band structure of the composite material is important for transporting carriers between QDs and perovskite NWs. The iodide
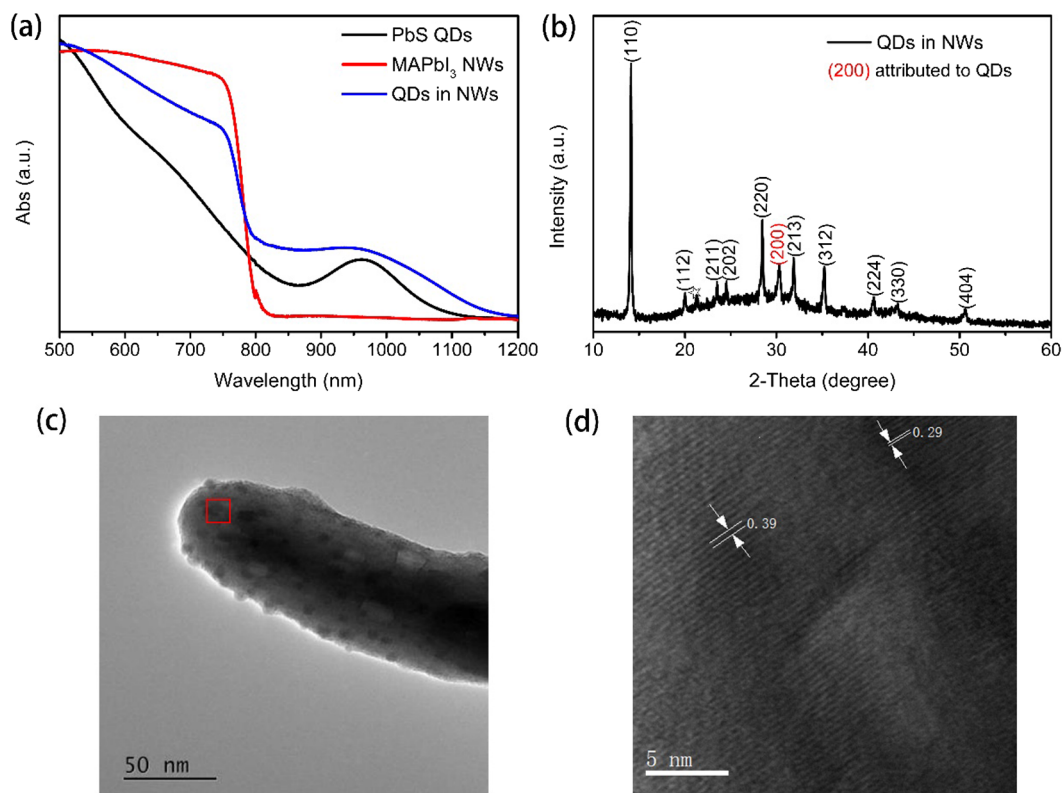
Fig. 3. Characterization of nanowires (a) Absorption spectra of PbS QD films, MAPbI$_3$ NWs and QDs in NWs, (b) X-ray diffraction pattern of QDs in NWs film, (c) Transmission electron microscope of a single nanowire, (d) High resolution image of nanowire (the red section in (c)). The mass ratio of PbS QDs to PbI$_2$ is 1:1 in b, c. (For interpretation of the references to colour in this figure legend, the reader is referred to the web version of this article.)

capped PbS QDs have a suitable band alignment with MAPbI$_3$ perovskites. The conduction band minimum (CBM) and valence band maximum (VBM) positions of iodide passivated PbS QDs ($\lambda_{excition}$ = ~950 nm) are around −5.5 eV and −4.2 eV, respectively [32]. The CBM and VBM positions for MAPbI$_3$ perovskites are −5.4 eV and −3.7 eV, respectively [33]. The higher CBM of perovskites facilitates electron transfer from perovskites into QDs, while the close VBM values allows hole transfer between the MAPbI$_3$ perovskites and QDs (Fig. 5d). However, it should be noted that the interface defects between QDs and perovskites could impede carriers transport between them [34].

We fabricated photodetectors based on a photoconductor structure growing NWs on gold contacts with a channel of 50 μm. The I-V curves tested in dark conditions show a deviation from Ohmic-like behavior at low voltages, possibly due to the formation of a junction between gold contacts and perovskite NWs. The current increases continuously with increasing illumination intensity (640 nm light source). The on/off ratio is ~2.5 when the illumination intensity increases to 30 mW (Fig. 5b). The responsivity is around 1–5 mA/W with the bias of −5 V and an irradiation of 640 nm (Fig. 6c). The small current at μA scale could be ascribed to the large channel between the contacts. The repeatability measurement was performed to test the stability of the device, as shown in Fig. 5c. No obvious photocurrent decay is observed after 10 cycles. The rise time and decay time extracted from the photocurrent curve (Fig. 6a) were 79.1 ms and 72.7 ms, respectively. The relatively slow response could be ascribed to defects related carrier recombination and low carrier mobility.

We then measured the performance of the photodetector under IR illumination. The QD-in-NW device showed a light response when

illuminated with 940 nm light, indicating that carriers generated within the QDs can transfer to perovskites (Fig. 6b, black curve). However, the photocurrent was low, which could be ascribed to the interface defects that impeded the electron transfer. To exclude the influence of the thermal induced current, a QD free nanowire control device was prepared; no light response with a 940 nm irradiation was observed, proving the IR response was indeed coming from the QDs (Fig. 6b, red curve). When there was no bias voltage, the photo-generated carriers could go through recombination between the QD and perovskite nanowire interface. When a moderate bias was applied (10 V), the photo generated carriers in PbS QDs could transfer along the electric field (Fig. 5e, f). It was proven that the electron in such a structure could escape from the QDs to perovskites through a field-assisted Fowler-Nordheim tunneling mechanism [20]. Photogating due to the accumulation of photocarriers in NWs could be another possible reason for the photocurrent [35].

In the end, as a proof of concept, a flexible device was fabricated on a polyethylene terephthalate (PET) substrate. The flexible device showed photoresponse when bent and the current increased under illumination (Fig. 6d). However, the photocurrent was still low, and further optimization to improve this device will be investigated in future work.

4. Conclusion

In summary, we fabricated a dot-in-wire nanocomposite with PbS QDs embedded in MAPbI$_3$ perovskite NWs. The use of DMF as a solvent induced the growth of NWs and the PbS QDs acted as seeds that
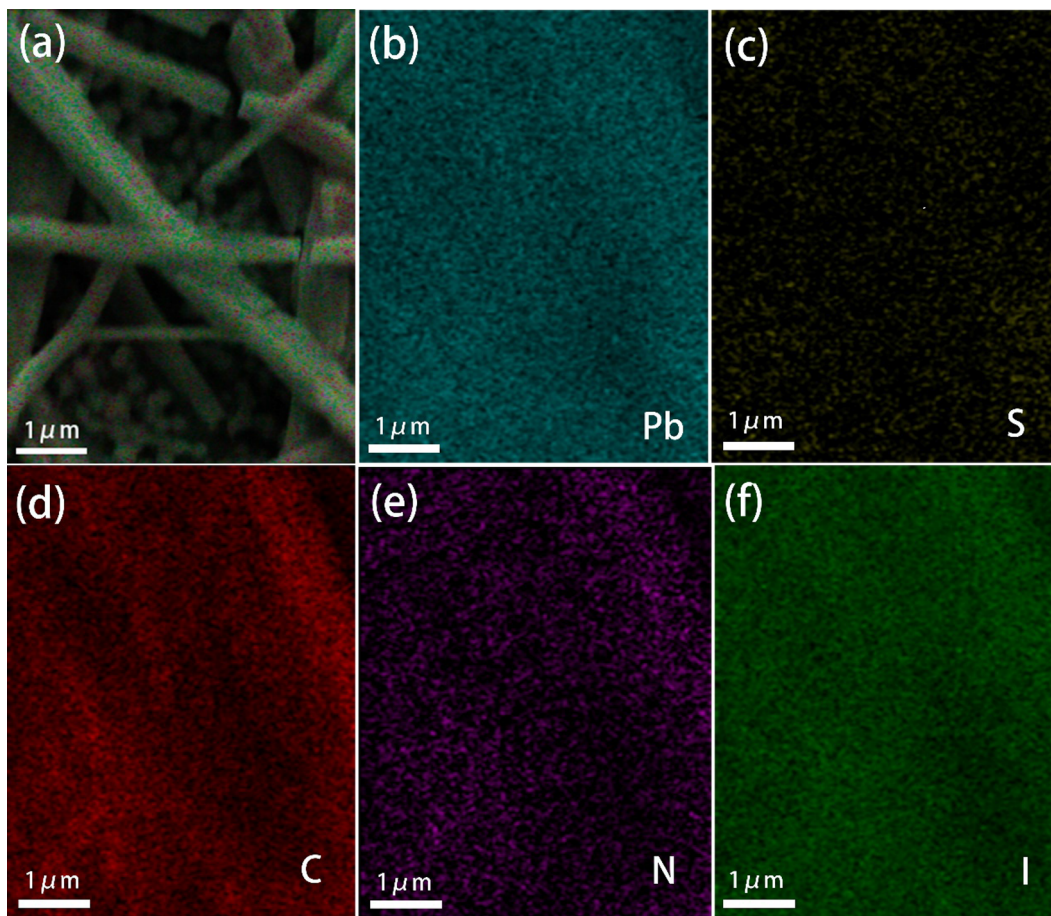
Fig. 4. Imaging of a dot-in-nanowire film, (a) Top-view SEM image, EDS mapping images of (b) lead, (c) sulfur, (d) carbon, (e) nitrogen and (f) iodine.
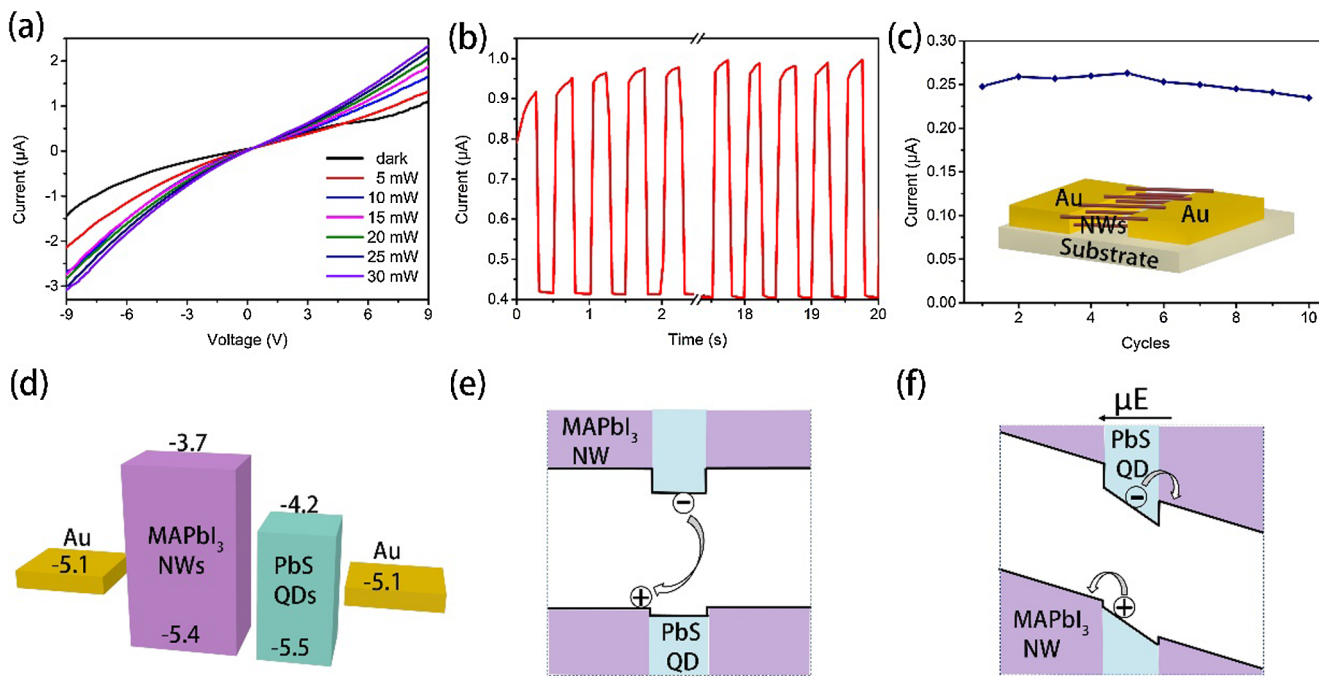

Fig. 5. Device performance illuminated by 640 nm light source, (a) I-V curves, (b) I-t curve, (c) Repeatability of photocurrent, inset is the schematic of the device structure, (d) Band alignment of dot-in-wire photodetector, (e) flat band state of a single PbS QD, (f) band alignment at a moderate voltage.
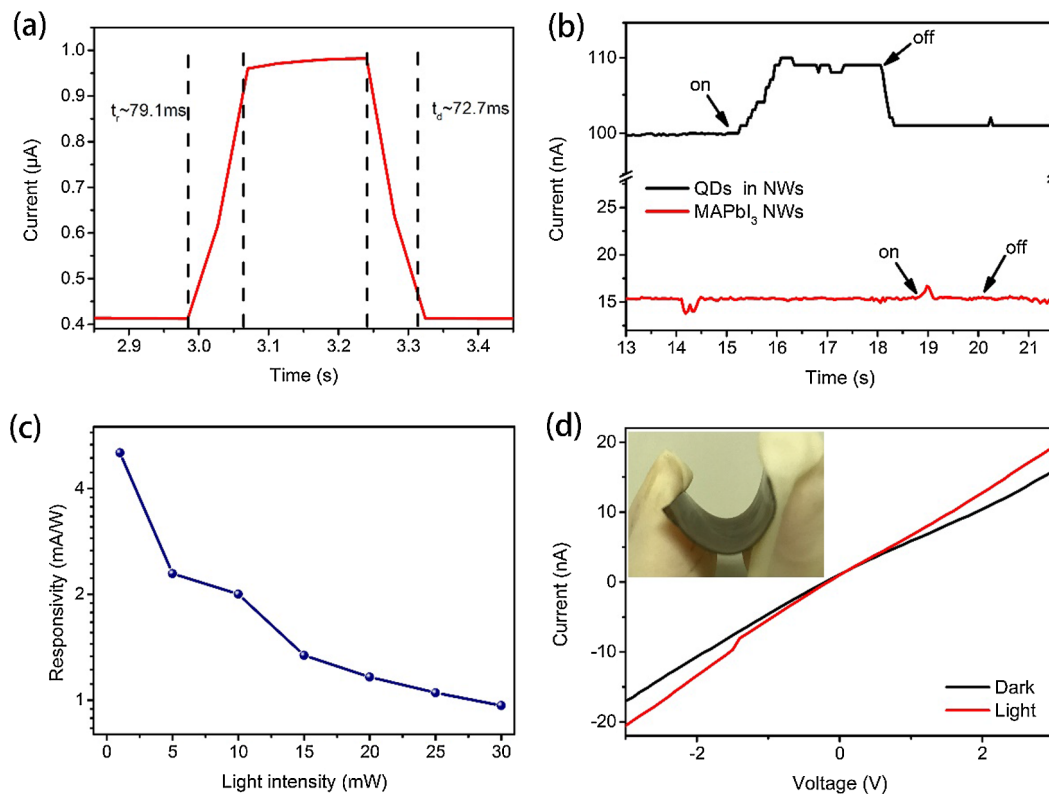
Fig. 6. Photodetector performance (a) Temporal response under 640 nm light source illumination, (b) Photocurrent curves of the photodetector with and without embedded QDs, illuminated by a 940 nm light source at a bias of 10 V, (c) Responsivity under different light intensities under the illumination of a 640 nm light source, (d) I-V curves of the device after bending under dark (black line) and illumination (red line). The inset is the photograph of the flexible photodetector on a PET substrate. (For interpretation of the references to colour in this figure legend, the reader is referred to the web version of this article.)

accelerated a uniform nanowire growth. Transmission electron microscopy revealed monodisperse PbS QDs embedded in MAPbI₃ NWs. Photodetectors based on this nanocomposite showed photoresponse in both visible and IR regions. This work expands the family of nanomaterials that can be utilized for IR photodetection.

Conflict of interest

The authors declare that we do not have any commercial or associative interest that represents a conflict of interest in connection with the work submitted.

Acknowledgements

References

[1] F. Xu, X. Liu, K. Fujimura, Pedestrian detection and tracking with night vision, IEEE T. Intell. Transp. 6 (2005) 63–71.

[2] S. Ioannou, V. Gallese, A. Merla, Thermal infrared imaging in psychophysiology: potentialities and limits, Psychophysiology 51 (2014) 951–963.

[3] M.R. Hasan, E.S. Arinze, A.K. Singh, V.P. Oleshko, S. Guo, A. Rani, Y. Cheng, I. Kalish, M.E. Zaghloul, M.V. Rao, N.V. Nguyen, A. Motayed, A.V. Davydov, S.M. Thon, R. Debnath, An antimony selenide molecular ink for flexible broadband photodetectors, Adv. Electron. Mater. 2 (2016) 1600182.

[4] L. Li, Z. Lou, G. Shen, Flexible broadband image sensors with SnS quantum dots/Zn₂SnO₄ nanowires hybrid nanostructures, Adv. Funct. Mater. 28 (2018) 1705389.

[5] M.-S. Park, M. Rezaei, I. Nia, R. Brown, S. Bianconi, C.L. Tan, H. Mohseni, InGaAs/InP quantum well infrared photodetector integrated on Si substrate by Mo/Au metal-assisted wafer bonding, Opt. Mater. Express 8 (2018) 413–419.

[6] M.V. Yakushev, V.S. Varavin, V.G. Remesnik, D.V. Marin, CdHgTe heterostructures on large-area Si(310) substrates for infrared photodetector arrays of the short-wavelength spectral range, Semiconductors 48 (2014) 767–771.

[7] G. Konstantatos, I. Howard, A. Fischer, S. Hoogland, J. Clifford, E. Klem, L. Levina, E.H. Sargent, Ultrasensitive solution-cast quantum dot photodetectors, Nature 442 (2006) 180–183.

[8] L. Zheng, W. Zhou, Z. Ning, G. Wang, X. Cheng, W. Hu, W. Zhou, Z. Liu, S. Yang, K. Xu, M. Luo, Y. Yu, Ambipolar graphene-quantum dot phototransistors with CMOS compatibility, Adv. Opt. Mater. 6 (2018) 1800985.

[9] Q. Xiong, F.I. Chowdhury, X. Wang, Filter-free narrowband photodetectors employing colloidal quantum dots, IEEE J. Sel. Top. Quant. 24 (2018) 1900406.

[10] R. Wang, X. Wu, K. Xu, W. Zhou, Y. Shang, H. Tang, H. Chen, Z. Ning, Highly efficient inverted structural quantum dot solar cells, Adv. Mater. 30 (2018) 1704882.

[11] F.P. García de Arquer, A. Armin, P. Meredith, E.H. Sargent, Solution-processed semiconductors for next-generation photodetectors, Nat. Rev. Mater. 2 (2017) 16100.

[12] H. Tang, J. Zhong, K. Wang, X.W. Sun, Methylammonium iodide (MAI) enhanced, solution processed high-performance photodetector based on lead sulfide quantum dots, SID Symp. Dig. Tech. Pap. 49 (2018) 108–111.

[13] Z. Ning, Y. Ren, S. Hoogland, O. Voznyy, L. Levina, P. Stadler, X. Lan, D. Zhitomirsky, E.H. Sargent, All-inorganic colloidal quantum dot photovoltaics employing solution-phase halide passivation, Adv. Mater. 24 (2012) 6295–6299.

[14] Y. Tang, F. Wu, F. Chen, Y. Zhou, P. Wang, M. Long, W. Zhou, Z. Ning, J. He, F. Gong, Z. Zhu, S. Qin, W. Hu, A colloidal-quantum-dot infrared photodiode with high photoconductive gain, Small 14 (2018) 1803158.

[15] E. Heves, Y. Gurbuz, Highly responsive, solution-based Al/PbS and Au-Ti/PbS Schottky photodiodes for SWIR detection, IEEE Sens. J. 14 (2014) 816–820.

[16] Q. Dong, Y. Fang, Y. Shao, P. Mulligan, J. Qiu, L. Cao, J. Huang, Electron-hole diffusion lengths > 175 μm in solution-grown CH₃NH₃PbI₃ single crystals, Science 347 (2015) 967–970.

[17] L. Hu, G. Shao, T. Jiang, D. Li, X. Lv, H. Wang, X. Liu, H. Song, J. Tang, H. Liu, Investigation of the interaction between perovskite films with moisture via in situ electrical resistance measurement, ACS Appl. Mater. Inter. 7 (2015) 25113–25120.

[18] F. Wang, X. Jiang, H. Chen, Y. Shang, H. Liu, J. Wei, W. Zhou, H. He, W. Liu, Z. Ning, 2D-Quasi-2D-3D hierarchy structure for tin perovskite solar cells with enhanced efficiency and stability, Joule 2 (2018) 1–12.

[19] X. Gong, Z. Yang, G. Walters, R. Comin, Z. Ning, E. Beauregard, V. Adinolfi, O. Voznyy, E.H. Sargent, Highly efficient quantum dot near-infrared light-emitting diodes, Nat. Photon. 10 (2016) 253–257.

[20] F.P. García de Arquer, X. Gong, R.P. Sabatini, M. Liu, G.-H. Kim, B.R. Sutherland, O. Voznyy, J. Xu, Y. Pang, S. Hoogland, D. Sinton, E. Sargent, Field-emission from

quantum-dot-in-perovskite solids, Nat. Commun. 8 (2017) 14757.

[21] D. Dong, H. Deng, C. Hu, H. Song, K. Qiao, X. Yang, J. Zhang, F. Cai, J. Tang, H. Song, Bandgap tunable $Cs_x(CH_3NH_3)_{1-x}PbI_3$ perovskite nanowires by aqueous solution synthesis for optoelectronic devices, Nanoscale 9 (2017) 1567–1574.

[22] W. Deng, L. Huang, X. Xu, X. Zhang, X. Jin, S.-T. Lee, J. Jie, Ultrahigh-responsivity photodetectors from perovskite nanowire arrays for sequentially tunable spectral measurement, Nano Lett. 17 (2017) 2482–2489.

[23] L. Gao, K. Zeng, J. Guo, C. Ge, J. Du, Y. Zhao, C. Chen, H. Deng, Y. He, H. Song, G. Niu, J. Tang, Passivated single-crystalline $CH_3NH_3PbI_3$ nanowire photodetector with high detectivity and polarization sensitivity, Nano Lett. 16 (2016) 7446–7454.

[24] D. Wu, H. Zhou, Z. Song, R. Liu, H. Wang, The effect of N, N-dimethylformamide on $MAPbI_3$ nanowires for application in flexible photodetectors, J. Mater. Chem. C 6 (2018) 8628–8637.

[25] Z. Yang, A. Janmohamed, X. Lan, F.P. García de Arquer, O. Voznyy, E. Yassitepe, G.-H. Kim, Z. Ning, X. Gong, R. Comin, E.H. Sargent, Colloidal quantum dot photovoltaics enhanced by perovskite shelling, Nano Lett. 15 (2015) 7539–7543.

[26] R. Wang, Y. Shang, P. Kanjanaboos, W. Zhou, Z. Ning, E.H. Sargent, Colloidal quantum dot ligand engineering for high performance solar cells, Energ. Environ. Sci. 9 (2016) 1130–1143.

[27] Z. Ning, X. Gong, R. Comin, G. Walters, F. Fan, O. Voznyy, E. Yassitepe, A. Buin, S. Hoogland, E.H. Sargent, Quantum-dot-in-perovskite solids, Nature 523 (2015) 324–328.

[28] A.A. Petrov, N. Pellet, J.-Y. Seo, N.A. Belich, D.Y. Kovalev, A.V. Shevelkov, E.A. Goodilin, S.M. Zakeeruddin, A.B. Tarasov, M. Graetzel, New insight into the formation of hybrid perovskite nanowires via structure directing adducts, Chem. Mater. 29 (2017) 587–594.

[29] P. Zhu, S. Gu, X. Shen, N. Xu, Y. Tan, S. Zhuang, Y. Deng, Z. Lu, Z. Wang, J. Zhu, Direct conversion of perovskite thin films into nanowires with kinetic control for flexible optoelectronic devices, Nano Lett. 16 (2016) 871–876.

[30] X. Guo, C. McCleese, C. Kolodziej, A.C.S. Samia, Y. Zhao, C. Burda, Identification and characterization of the intermediate phase in hybrid organic–inorganic $MAPbI_3$ perovskite, Dalton T. 45 (2016) 3806–3813.

[31] Y. Kim, M. Chang, B. Park, Near infrared-induced optical gating at the lead-sulfide (PbS)/pentacene interface, Thin Solid Films 651 (2018) 85–90.

[32] C.-H.M. Chuang, P.R. Brown, V. Bulović, M.G. Bawendi, Improved performance and stability in quantum dot solar cells through band alignment engineering, Nat. Mater. 13 (2014) 796–801.

[33] S. Wang, T. Sakurai, W. Wen, Y. Qi, Energy level alignment at interfaces in metal halide perovskite solar cells, Adv. Mater. Interf. 5 (2018) 1800260.

[34] J.M. Azpiroz, E. Mosconi, J. Bisquert, F. De Angelis, Defect migration in methylammonium lead iodide and its role in perovskite solar cell operation, Energ. Environ. Sci. 8 (2015) 2118–2127.

[35] H. Fang, W. Hu, Photogating in low dimensional photodetectors, Adv. Sci. 4 (2017) 1700323.